Revision submitted to Journal of Neurophysiology

Evidence from Retractor Bulbi EMG for Linearised Motor Control of Conditioned Nictitating Membrane Responses

N.F.Lepora[1], E.Mavritsaki[2], J.Porrill[1], C.H.Yeo[3], C.Evinger[4], P.Dean[1]

[1]*Department of Psychology, University of Sheffield, Western Bank, Sheffield S10 2TP, U.K.*

[2]*School of Psychology, University of Birmingham, Edgbaston, Birmingham B15 2TT, U.K.*

[3]*Department of Anatomy and Developmental Biology, University College London, Gower Street, London WC1E 6BT, U.K.*

[4]*Department of Neurobiology & Behavior, SUNY, Stony Brook, NY 11794-5230, USA*

Running Head: Linearised conditioned eyeblink responses

Correspondence to: Paul Dean, Department of Psychology, University of Sheffield, Western Bank, Sheffield S10 2TP, U.K. E-mail: p.dean@sheffield.ac.uk Phone: +44 114 222 6521 Fax: +44 114 276 6515

ABSTRACT

Classical conditioning of nictitating membrane (NM) responses in rabbits is a robust model learning system, and experimental evidence indicates that conditioned responses (CRs) are controlled by the cerebellum. It is unknown whether cerebellar control signals deal directly with the complex non-linearities of the plant (blink-related muscles and peripheral tissues), or whether the plant is linearised to ensure a simple relation between cerebellar neuronal firing and CR profile. To investigate this question, the retractor bulbi muscle EMG was recorded with implanted electrodes during NM conditioning. Pooled activity in accessory abducens motoneurons was estimated from spike trains extracted from the EMG traces, and its temporal profile found to have an approximately Gaussian shape with peak amplitude linearly related to CR amplitude. The relation between motoneuron activity and CR profiles was then accurately fitted by a first order, linear filter, with each spike input producing an exponentially decaying impulse response with time constant of order 0.1 s. Application of this first-order plant model to CR data from other laboratories suggested that in these cases also motoneuron activity had a Gaussian profile, with time-of-peak close to unconditioned stimulus (US) onset and standard deviation proportional to the interval between conditioned stimulus and US onsets. These results suggest that for conditioned NM responses the cerebellum is presented with a simplified 'virtual' plant that is a linearised version of the underlying non-linear biological system. Analysis of a detailed plant model suggests that one method for linearising the plant would be appropriate recruitment of motor units.

INTRODUCTION

Classical conditioning of the external eyelid blink and, in rabbits, the nictitating membrane response (NMR) is widely studied as a model learning system, and a wide variety of evidence indicates that the cerebellum is essential for the production of conditioned responses (CRs) of the external eyelids and of the nictitating membrane (Hesslow and Yeo 2002; Thompson 2005). Nonetheless, the nature of the control signal sent from the cerebellum to the relevant motoneurons is still unclear. Initial data from multi-unit recordings in the interpositus nucleus (McCormick and Thompson 1984) indicated a firing rate profile that simply mimicked the profile of the conditioned NMR. Consequently, many models of the cerebellum in eyeblink conditioning essentially stop at the interpositus nucleus, with no representation either of efferent target neural populations such as the red nucleus and motor nuclei, or of the plant itself. (Balkenius and Morén 1999; Fiala et al. 1996; Garenne and Chauvet 2004; Gluck et al. 2001; Hofstötter et al. 2002; Medina and Mauk 2000; Moore and Choi 1997). (The term plant refers to 'that which is controlled', in this case by the signal sent from the motoneurons, and corresponds to the relevant muscles together with orbital or eyelid tissue). Nevertheless, the assumption that the plant has very simple dynamics is not obviously true, and has been questioned explicitly: "... it is somewhat unlikely that the actual discharge rate of interpositus neurons could be correlated with the profile of CRs determined from nictitating membrane displacement, as this is a passive, highly damped movement" (Delgado-García and Gruart 2005, p.375). The question is to what extent the system peripheral to the interpositus nucleus presents the cerebellum with complex non-linear control problems that must be taken into account in order to produce appropriately timed and shaped conditioned eyeblink responses.

Part of the answer to this question has been provided by a detailed model of a portion of the peripheral system (Bartha and Thompson 1992a; 1992b). This model relates the firing patterns of accessory abducens motoneurons to the NMR, describing the detailed mechanism by which contraction of the retractor bulbi (RB) muscle retracts the globe, displacing Harder's gland and thus forcing the nictitating membrane across the cornea (Eglitis 1964). The model is also consistent with Lennerstrand's (1974) recordings of RB isometric force as a sigmoidal function of input frequency with only a narrow linear range. A subsequent re-implementation of this model (Mavritsaki et al. 2007) has identified two main sources of nonlinearity. The first non-linearity originates from the sigmoidal pattern

in muscle force, which is reproduced in the NMR itself if the system uses rate coding as a control strategy (Mavritsaki et al. 2007, Fig 8). In rate coding, all units fire with the same frequency, and force increases occur by increasing frequency. The second major non-linearity was observed when the system used a simple recruitment control strategy in which units (all of equal strength) either did not fire, or fired with a fixed frequency. In this strategy force is increased by increasing the number of units firing. However, increasing the number of active motor units also increases muscle stiffness, so that the equilibrium position of the muscle in relation to an elastic load increases sublinearly with the number of units recruited (Mavritsaki et al. 2007, Fig 9). The presence of these clear non-linearities suggests that concerns about plant complexity (Delgado-García and Gruart 2005) are entirely justified, and appear to preclude any simple relation between control signal and NMR.

However, it also proved possible to use the model to demonstrate that there were recruitment strategies capable of producing a linear relation between summed motoneuron activity and NMR amplitude. One was an appropriate combination of rate-coding with recruitment (Mavritsaki et al. 2007, Fig 10); the other was recruitment of motor units of appropriately increasing strength (Mavritsaki et al. 2007, Fig 11). These strategies in effect produce a simplified 'virtual plant' that is easier to control, because its input signals are restricted to a set over which the plant appears linear, while still maintaining the full response range of the system. Thus, for example, doubling output amplitude can be achieved merely by doubling the amplitude of the input signal, without concern for nonlinear effects such as response saturation. The existence of appropriate recruitment strategies means that the presence of substantive non-linearities in the output systems peripheral to the interpositus nucleus does not necessarily invalidate the simple models of cerebellar control referred to above. Furthermore, the presentation to the cerebellum of a simple virtual plant in the case of NMR conditioning would be suggestive of a more general operating principle whereby physiological output systems are structured to simplify the task of neural control (e.g. Angelaki and Hess 2004; Mussa-Ivaldi et al. 1994; e.g. Nichols and Houk 1976).

One way of testing for this simplified virtual plant is to examine the relationship between the firing of accessory abducens motoneurons and the characteristics of conditioned NMRs. Existing data on this relationship are, however, sparse. Single unit studies in rabbit have been very preliminary (Berthier and Moore 1983; Disterhoft et al. 1985; Disterhoft and Weiss 1985), and one study suggests that such motoneurons fire only in relation to unconditioned NMRs in the cat (Trigo et al. 1999). An

early study of multi-unit motoneuron firing in rabbit showed activity profiles that strongly resembled, and were highly correlated with, the time-course of the NMR (Cegavske et al. 1979, Fig 8), suggesting that "[w]hatever the abducens units do, so will the NM do" (p.605). Nevertheless, the recordings were from the abducens rather than accessory abducens, only four examples of relevant data were shown, and no explicit demonstration of linearity was undertaken. The present study therefore sought to obtain more data on the relation between firing in the accessory abducens motoneuron pool and NMR dynamics, by recording the EMG from the retractor bulbi muscle during the production of conditioned NMRs, and analyzing the EMG records to estimate the occurrence of motor unit action potentials (Gruart et al. 1995; Sanders et al. 1996). Because of the technical difficulties of electrode implantation in this muscle in combination with the recording of NM position during conditioning, the present results constitute, to the best of our knowledge, the first systematic description of retractor bulbi EMG during conditioning. Portions of the findings have been presented previously in abstracts (Lepora et al. 2005; Mavritsaki et al. 2001).

METHODS

Data Collection

Data were obtained from two different laboratories, one at University College London (Yeo) and the other at the State University of New York at Stony Brook (Evinger).

UCL Procedures

For adaptation and training, each subject was placed in a restraining box in a sound attenuating chamber facing a centrally mounted loudspeaker, and the NM transducer fitted. In the 50 min adaptation session, no stimuli were presented. For acquisition, the conditioned stimulus (CS) was a 1 kHz sinusoidal tone of intensity 85 dbA and duration 410 msec (RB2, RB3) or 560 ms (RB1), delivered through the loudspeaker. The unconditioned stimulus (US) was a 60 ms train of 3 biphasic current pulses of 2 mA delivered to the periorbital region. The inter-trial interval between CS presentations varied randomly between 25 and 35 s, and 100 trials were presented each session. On every 10th trial the CS was presented alone. On each trial EMG and NMR data were recorded for a 2 sec period starting 1 sec before CS onset. EMG data were sampled at 5-40 kHz and NMR data at 1kHz. After acquisition, RB1 and RB2 were tested with triplets in which one trial was CS alone, one CS+US, and one US alone. In addition, RB1 was tested with varying CS intensities (65, 75, 85 and 95 dBA).

SUNY Procedures

After initial acquisition of the conditioned response, RB4 was tested under a variety of conditions, including variations in CS and US intensity, and extinction. RB5 was tested with variations in CS intensity only.

Data Analysis

Data Selection

The data used for analysis came from trials in which the CS was presented on its own, and CR amplitude was >2.5% of the maximum CR amplitude for that subject. About 15 % of these trials were subsequently discarded because there was spontaneous movement of the NM just before CS

presentation, or there was interference in the EMG or NMR signals, or there was evidence from the EMG recording suggesting that the electrode moved during the CR.

EMG Analysis

Figure 1 about here

As explained in the Introduction, the method of analysis adopted here was to estimate the occurrence of motor-unit action potentials from spikes in the EMG records from the intramuscular electrodes (Sanders et al. 1996). The procedure chosen was the simple one of threshold crossing, that is whenever the EMG record increased past a threshold, θ, a spike was registered (Fig 1A). Given an EMG signal $x = (x_0, x_1, x_2, \ldots)$ sampled at frequency f_s Hz, [i.e. at discrete times $t=(0, 1/f_s, 2/f_s, \ldots)$], this procedure gives a spike sequence, s, that is a binary signal of zeros and ones

$$s = (s_0, s_1, s_2, \cdots), \qquad s_i = \begin{cases} 1, & x_i < \theta < x_{i+1}, \\ 0, & \text{otherwise.} \end{cases} \tag{1}$$

Where necessary, EMG traces were subsampled at 5 kHz to eliminate multiple-spike counting artifacts caused by high-frequency noise..

One potential problem with the above procedure is that at high frequencies spikes begin to overlap, producing what is termed an interference pattern (Sanders et al. 1996). To estimate the possible effect of such overlap on estimates of spike frequency, we compared the results of (i) summing different EMG records and extracting spikes to (ii) extracting spikes from the individual records and summing them. At frequencies where spike interference is significant, the number of extracted spikes from the summed EMGs will be less than the sum of the spikes from the individual EMGs. Our results indicated that the spike frequency at which interference became appreciable was dataset dependent (RB1 = 400 spikes/s, RB2 = 350 spikes/s, RB3 = 400 Spikes/s and RB4 = 550 spikes/s). The dataset dependence appeared to arise from differences between data sets in the width of the EMG spikes. Our observed frequency ranges almost always lay below the interference frequency (peak frequency of RB1 = 450 spikes/s, RB2 = 225 spikes/s, RB3 = 425 spikes/s and RB4 = 350 spikes/s). There may however have been some interference effects for a small number of RB1 and RB3 recordings. However, these records comprise a small proportion of the available data, and no appreciable biasing was observed in our analysis.

A second potential problem with our method of analysis concerns choice of threshold θ for each subject, which was complicated by variability in the EMG records between trials, possibly the result of electrode movement produced by muscle contraction. The main kinds of variability are fluctuations in general sensitivity (both spike size and background noise changed), or the apparently random appearance of tonic spikes clearly unrelated to the CR, possibly originating in adjacent extraocular muscles. This is a classic signal to noise separation problem, which can only be solved by explicit choice of a criterion for separating signal and noise. Our criterion was an EMG threshold for each subject such that, for all of the trials used in the analysis, there was neither a bias towards trials where EMG spikes occurred without a corresponding CR (threshold too low) nor towards trials where no EMG spikes occurred but a CR did (threshold too high). Presence of a CR depended upon whether the NMR passed 0.1mm amplitude. Further details are given below in the section on Response Linearity.

Once spikes had been extracted, their frequencies were calculated from the number of spikes in a 10 ms time interval. The noise levels of individual records usually meant that data had to be pooled across trials based on CR amplitude. Since the initial part of the resulting frequency profiles appeared to resemble a normal distribution (see Results), they were fitted with a Gaussian bell-shaped curve with the equation

$$g(t) = h \exp\left[\frac{-(t-\mu)^2}{2\sigma^2}\right], \tag{2}$$

where $g(t)$ is the value of the curve at time t, μ is time corresponding to the mean of the distribution, h its height and σ a measure of its width. These parameters were estimated from the frequency dataset as follows.

(i) The mean is the mean of all the times at which spikes occur, given by

$$\mu = \frac{1}{N}\sum_{i=1}^{n} f_i\, t_i, \qquad N = \sum_{i=1}^{n} f_i, \tag{3}$$

where f_i represents the frequency of the ith bin from a total of n bins and t_i is the time at which that frequency occurs (*e.g.* t_i=50i−25 ms for n=20 bins of a 2 s record).

(ii) Height h is the peak value of the frequency dataset.

(iii) The width σ is found by equating the spike total of the frequency dataset to that for the Gaussian curve (*i.e.* matching areas under the curves). A well-known mathematical identity then gives

$$\sigma = \frac{1}{h\sqrt{2\pi}} \int_{t=0}^{2} g(t)\, dt = \frac{1}{h\sqrt{2\pi}} \sum_{i=1}^{n} f_i\, \delta = \frac{N\delta}{h\sqrt{2\pi}}, \qquad (4)$$

where δ = 50 ms is the width of the frequency bin.

Fitting was restricted to the interval from CS onset to one ISI after US onset (ISI = interstimulus interval, that is time between CS and US onsets), to exclude a tail in the frequency profile of some records. This range actually covers most of the frequency variation of each record, because the peak frequency typically occurs significantly before US onset (see Fig. 4, for example).

Response Linearity

Response linearity was assessed in two ways. First, the relation between peak CR amplitude and peak EMG frequency was examined. For a given subject, the records from individual trials were sorted on the basis of CR amplitude, and averaged over a suitable trial range to reduce the effects of noise (a range of 3 trials gave a good balance between reducing noise and choosing similar records – see below). Each group of records contributed a point to a scatterplot of peak CR amplitude against peak EMG frequency. The best linear and quadratic fits to these points were then determined for each subject, using standard statistical techniques. The fits were determined for a range of thresholds for EMG spike extraction (see above). This threshold choice does not depend on fit linearity, since linearity and intersecting a given point are independent measures. The threshold chosen was the one that gave a line of best fit which passed through the origin. This choice was based on the criterion that too high a threshold would give examples of CRs without any EMG spikes, and too low a threshold EMG spikes without any CRs (see above). In fact the goodness of the linear fit was typically similar over a wide range of threshold values (Fig 5E), reinforcing the point that this method of choosing the threshold did not bias the analysis in favor of linearity.

The second method of investigating response linearity was to determine the best-fit linear filter that related instantaneous EMG frequency to CR amplitude. (The signal-processing term 'filter' describes the transformation of a time-varying input signal to a time-varying output signal. In biological or electrical systems, for example, these transformations often involve processes that can be represented by linear differential equations.) Since initial analysis with filters of increasing complexity

indicated that for each subject the data could be well fitted with a first-order filter, the fitting procedure is described for the first-order case. A first order filter has a gain (*g*) and time constant (t_0). A unit impulse input to the filter produces an instantaneous response of height *g* which decays exponentially with time constant t_0. The filter output y_i at the *i*-th time step is related both to its output y_{i-1}at the preceding time step and to the current spike input *s* by the difference equation

$$y_i = b\, s_i - a\, y_{i-1}\,, \tag{5}$$

where $b = g/f_s$, $a = -\exp(-1/f_s t_0)$, and f_s is the sampling frequency (corresponding to $1/\Delta t$ where Δt is the time step). The form of equation (5) is well known from signal processing theory, and it can be seen heuristically that it gives the impulse response appropriate for a first-order filter because the *bs* term drives a response that is a multiplicative gain *b* of the spike input while the ay_{i-1} term makes this response exponentially decay over the following time steps. A system latency between the spike inputs and NM response can also be included in the model by delaying the input signal by an appropriate number of time steps. For a latency λ seconds the signal *s* is delayed by $d=f_s\,\lambda$ time steps, giving the difference equation

$$y_i = g\, s_{i-d} - a\, y_{i-1} \tag{6}$$

Estimating the best-fit first-order filter therefore requires estimating values for the three parameters λ, *g* and t_0.

The latency was estimated directly from the data. Examining the start points of the EMG and NM response data showed the latency was typically between 10 and 30 ms for each trial of all datasets with a mean of 20 ms, values which probably reflect the highly damped nature fo the plant (Mavritsaki et al. 2007). A sensitivity analysis showed our results did not depend appreciably on the particular value in this observed range, and so the value λ =20 ms was used. The parameters *g* and t_0 were estimated by regression analysis, using as an estimate for the fit error the standard RMS difference between the predicted output *y* from equation (6) and the measured output y_{data},

$$e = \sqrt{\left\langle \left(y - y_{\text{data}}\right)^2 \right\rangle} = \sqrt{\frac{1}{n+1}\sum_{i=0}^{n}\left[y_i - \left(y_{\text{data}}\right)_i \right]^2}\,, \tag{7}$$

where *n* was the number of samples in the dataset. Equation (7) is the fit error for a single trial: for the whole dataset the RMS fit error over all *N* trials was used, with $\hat{e} = \sqrt{\left\langle \left(e_1, \cdots, e_N\right) \right\rangle}$ where e_j was the

fit error of the *j*-th trial. The best fit is then found by minimizing the dataset error $\hat{e}$ over the parameters *g* and t_0. This optimization is achieved with a standard gradient descent algorithm. The overall quality of the fit can then be described with the nonlinear regression coefficient,

$$R^2 = 1 - \frac{SS(y - y_{\text{data}})}{SS(y_{\text{data}})}, \quad . \tag{8}$$

where *SS* denotes sum of squares, y_{data} the set of data points, and $y\text{-}y_{data}$ the set of differences between predicted values *y* and the data points. A value of R^2 close to one indicates that the best model fit represents the data well.

Modelling

Detailed Model

The detailed model of the relation between motoneuron firing and conditioned NMR used in the present study was that described in Mavritsaki (2007), which is based closely on a previous model of Bartha and Thompson (1992a; 1992b). The inputs to the model are the firing rates of 100 simulated motoneurons, and its output is instantaneous NM position (Fig 7). Three processes are represented explicitly: (i) the production of isometric force by a motor unit in the retractor bulbi in response to its input train of motoneuron action potentials; (ii) the conversion of this notional force to actual force taking into account the muscles position and velocity; and (iii) the action of this force on the mechanics of globe retraction and Harder's gland compression. In the linearised model used here, motoneurons are recruited as the input signal to the motoneuron pool increases and in addition increase their firing rates (details in Mavritsaki et al. 2007). The model was run with a time step of 1 ms, and the output smoothed by taking a 50 ms running average of the simulated isometric force, plotted every 1 ms.

Simple Model

This model is derived from the observation that the relation between EMG spikes and conditioned NMRs can be approximated by a first-order filter. The discrete time version of such a filter is given by equation (5) that relates amplitude y_i to the spike input s_i at discrete time t_i, given here in more convenient form

$$y_i - e^{-1/f_s t_0}\, y_{i-1} = g f_s\, s_i \ , \tag{9}$$

where g is the gain, t_0 the decay time constant and f_s is the sampling frequency. The continuous time analogue of this discrete time model corresponds to the limit of infinite sampling frequency $f_s \to \infty$, with

$$\frac{y_i - y_{i-1}}{\Delta t} + \frac{1}{t_0} y_{i-1} + O(\Delta t) = \left(\frac{g}{\Delta t} \right) s_i , \qquad \Delta t = 1/f_s . \tag{10}$$

Taking $\Delta t = 1/f_s \to 0$, gives the differential equation for this continuous time model

$$\dot{y}(t) + \frac{1}{t_0} y(t) = g\, s(t) . \tag{11}$$

The system is again linear and first order with gain g and time constant t_0.

Equation (11) can be interpreted as a notional muscle force F acting on a first-order viscoelastic plant

$$F = c\dot{y} + ky = c\left(\dot{y} + \frac{y}{t_0} \right), \tag{12}$$

with elasticity k and viscosity c giving a time constant $t_0 = c/k$. On the right-hand side of equation (11), averaging $s(t)$ over a time bin of T seconds gives an average spike frequency

$$\hat{f}(t) = \frac{1}{T} \int_{\tau=t}^{\tau=t+T} d\tau\, s(\tau) = \frac{1}{T} \sum_{t \le t_i \le t+T} s_i . \tag{13}$$

Therefore the continuous time model (8) is equivalent to stating that the notional muscle force is proportional to spike frequency

$$\frac{\hat{F}}{c} = g\, \hat{f} , \tag{14}$$

where both $\hat{F}$ and $\hat{f}$ are averaged over the same time interval T. The relation (14) gives an alternative method for qualifying whether the data is consistent with a first order, linear system. Estimates of the time constant t_0 can be obtained from the filter fit described above in the section on Response Linearity. This specifies F/c from the NM response amplitude $y(t)$.

To summarise, the above equations describe a simplified plant model that can be used (a) to predict instantaneous NM displacement from motoneuron firing rates, and (b) to estimate notional muscle forces and hence input frequencies from NMR profiles.

RESULTS

The results are presented in two sections. The first main section describes the data for subjects RB 1-4, and their analysis and modelling. The second brief section deals with two additional observations, (i) an analysis of data from subject RB5, and (ii) a lack of evidence for oscillations in conditioned NMR temporal profiles.

Data for RB 1-4.

Retractor Bulbi EMG and Conditioned NMRs.

Because there is little previous information available on retractor bulbi EMG and conditioned NMRs in rabbits, we first describe some basic features of the data. Fig 1A shows an example of spike extraction from the retractor bulbi EMG, from subject RB4. The full EMG and spike records for that trial, together with the corresponding conditioned NMR, are shown in Fig 1B. It can be seen that the peak of the CR occurs just before US onset (dotted vertical line, 350 ms after CS onset) whereas the EMG signal, which starts about 170 ms after CS onset, is almost finished by time of US onset. This record also illustrates why selecting an appropriate spike threshold is not straightforward (see Methods) if some of the spikes that are part of the 'noise' (i.e. unrelated to the CR) are larger than some of the spikes that are part of the 'signal' (i.e. related to the CR). Finally, it is apparent from both panels in Fig 1 that an extracted spike can correspond to excursions of different amplitude in the original EMG. These amplitude differences are ignored in present analysis, where all spikes are treated as equal, but will be the subject of a subsequent report on possible recruitment of motor units in the retractor bulbi muscle.

Figure 2 about here

In order to examine the frequency profiles of the extracted spike records, it proved necessary to pool data across records to reduce the often substantial variability between individual trials. For the examples shown in Fig 2, data were averaged for each subject over the largest 20% of its CRs and corresponding EMG spike frequency profiles. In all subjects the CR peak was close to US onset (range 28 ms before to 23 ms after), with peak EMG frequency 45-75 ms earlier than CR peak. The main differences between the subjects were (i) the values of CR amplitude, which ranged from 2-6 mm; (ii) the values of EMG peak frequency, which ranged from 200-400 spikes/s, possibly reflecting

the number of motor units that were sampled by the electrode; and (iii) how quickly the NM returned to its resting position. It can be seen that this return, which also appears in the recordings of conditioned NMRs from other laboratories (cf Fig 10A), was fastest in RB2 and 4, and much slower in RB 3. The relationship of this response 'tail' to EMG activity is not straightforward: there is prolonged EMG activity in the case of subject RB3, but not for RB1 although both subjects have substantial NMR 'tails'. This lack of relationship may arise because of EMG sampling problems when only few units are active, a view consistent with the irregular appearance of prolonged EMG discharge from trial to trial in subject RB3 (cf Figs 2 and 4). Tonic activity in the retractor bulbi EMG continuing after the conditioned response has also been observed in a study of eyelid conditioning (Leal-Campanero et al. 2004).

Figure 3 about here

To characterize the signals that control conditioned NMRs, it is important to know how both motoneuron activity and response profile vary with response amplitude. The variation for CRs is shown in Fig 3. Although in certain cases the traces were still quite noisy even after pooling across sets of 3 responses, it can be seen that the change in shape with amplitude is relatively slight, and much less pronounced than the differences in shape between subjects.

Figure 4 about here

This was also true for EMG spike frequency profiles (Fig 4), though in this case the differences between subjects were not as marked as for CR profiles. An important feature of the EMG frequency profiles was that they could be well fitted by Gaussian curves (see methods) over the time period starting at CS onset and continuing for twice the duration of the IS1 (time period equals 1 s for RB1, 0.7 s for the RB 2-4). Although the timing of the peak of the fitted Gaussians varied relatively little within subjects, there was a slight tendency for larger EMG signals to have earlier peaks. It should be noted that these Gaussian fits are entirely empirical, that is they do not depend upon any prior assumptions of system linearity, and they are significant not only for indicating the actual temporal profile of motoneuronal activity during CRs, but allowing it to be approximated by just three parameters (time and height of peak, and width - cf Figs 10 and 11).

EMG Spikes Linearly Related to Conditioned NMR

Because the inputs to the system as indicated by EMG spike frequency profiles have roughly similar shapes independent of their amplitude, it is possible to exploit the principle of superposition to test for linearity without knowing the exact relation between input and output. If input and output are linearly related, and the temporal profile of the input is invariant, then peak output should be directly proportional to peak input. Fig 5 shows this to be a reasonable approximation for the present data, with straight line fits giving r^2 values of 0.79 - 0.94. For each subject the data points were scattered around the straight line in a manner suggesting a noisy rather than a systematically nonlinear relation between the two variables. In fact fitting a quadratic curve to the data gave very little improvement in the proportion of variance accounted for (range 0 to 3% improvement) when both quadratic and linear fits were constrained to pass through the origin. In a further test of robustness, the datasets were fitted with straight lines using different values for the threshold for spike extraction (see Methods). There was typically a broad range of thresholds that gave good linear fits (Fig 5E). This is important in indicating that the method for selecting the threshold value, i.e. that value which gave a line of best fit that passed through the origin, did not bias the subsequent analysis towards linearity.

Figure 5 about here

Given the above evidence for overall linearity between input and output, the next step was to search for the linear filter that would give the best fits to the temporal profiles of the responses. As indicated in Methods, it turned out that a first order filter was adequate. Typical fits produced by such a filter are shown in Fig 6, which shows trials with the median fits (as determined by R^2, the proportion of variance accounted for) for filter fits over the whole dataset pooled over 3 trials. Given the noisiness of the data and the fact that the EMG spikes were a only a sample of total motoneuron activity, the fits shown in these panels (R^2 = 0.90-0.97) suggest that a first order filter is a reasonable approximation of the relationship between EMG spike input and conditioned NMR output.

Figure 6 about here

To check for overfitting in our analysis, we repeated the above procedure with separate fitting and validation sets. Filter fits were determined on the central 50% of trials (ordered by NMR peak amplitude) and goodness of fit determined on the outer 50% of trials. Parameter and fit values (R^2=0.90-0.98) were consistent with the above method.

Modelling

A detailed model of the relation between the firing rates of motoneurons in the accessory abducens nucleus and the displacement of the nictitating membrane (Fig 7) has been described by Bartha and Thompson (1992a; 1992b). This model includes a number of features which result in that relation being nonlinear. The first issue addressed in this section, therefore, is how the current results could be at all compatible with the detailed model. The second issue is the extent to which a much simpler linear model, based on the linear filter described above, can account both for the present data and for other published data on the temporal profiles of conditioned NMRs.

Figure 7 about here

Detailed Model

Bartha and Thompson's detailed model is organized into three parts (Fig 7), with the first describing the production of isometric force by an individual motor unit, the second deriving the actual force from isometric force using the muscle's length and velocity, and the final part calculating the instantaneous position of the NM as a function of the actual force. A subsequent implementation of this model (Mavritsaki et al. 2007) showed that its behavior depended critically on the nature of the control signals sent by the motoneuron pool. For simple rate-coding, in which muscle force is determined only by variations in the frequency with which all the units fire, there is a non-linear, sigmoidal, relationship between firing frequency and NMR amplitude (Mavritsaki et al. 2007, Fig 8), which reflects the relationship between the firing frequency and isometric force of a single motor unit (Lennerstrand 1974).

Figure 8 about here

However, it was possible to show that if motoneuron recruitment were combined in a suitable manner with frequency modulation, then the model behaved in a much more linear fashion (Mavritsaki et al. 2007, Fig 10). The response of this linearised version of the model to Gaussian-shaped frequency profiles inputs is shown in Fig 8A. It can be seen that peak NMR amplitude is linearly related to peak input frequency. The best-fit linear filter for this version of the model can be estimated from input-output data with the same techniques as those used for the actual data (Methods), and an example of filter performance is shown in Fig 8B. The CR output of the detailed model (labeled 'biophysical model' in Fig 8B) is approximated by the output of the linear filter (with time constant of

0.1 s and gain of 0.12). Thus, the present data showing a simple relation between EMG spikes and CR profiles can be consistent with a detailed model of the retractor bulbi muscle and associated plant. It is important to note that although recruitment is one way of improving the model's linearity, it is not necessarily the only way, so that the results illustrated in Fig 8 do not prove that the real system does use recruitment. This point is addressed further in the Discussion.

Linear Model

As indicated in Fig 6 the relationship between EMG spikes and conditioned NMRs can be approximated by a linear filter suggests a simple linear model of CR production, in which the summed motoneuron frequency profiles signal desired muscle force, and this force acts on a first order plant (Fig 7, bottom row). A simple test of such a model is to run the temporal profiles of a CR back through the first-order plant to estimate the force. In practice this was achieved by using the time constant t_0 of the fitted filter (values given in the legend to Fig 6) to construct the force $F \propto \dot{y} + y/t_0$ from equation (12). This estimated force can then be compared with the frequency profile of the associated EMG to verify they are linearly related, as assumed by the model equation (14).

Figure 9 about here

For the present data sets, peak EMG frequencies and estimated peak forces were linearly related (data not shown: r^2 range 0.80-0.94). Fig 9 shows records with median goodness of fits for data pooled over 3 trials. The reasonable fits between the actual EMG and inferred force profiles are consistent with the simplified model in which muscle input and force are related by a gain term only. It is of interest that this simple model gives a relationship between the firing rate *FR* of the motoneuron pool and NM position *y* and velocity *dy/dt*

$$FR = Ky + R\frac{dy}{dt} \tag{15}$$

similar to those observed for individual ocular motoneurons in relation to eye position and velocity.

Figure 10 about here

The above result, using the simple model in inverse mode, primarily confirms the result obtained when the model was used in forward mode (Fig 6). Moreover, the result also implies that the simple model can be used to reconstruct summed motoneuron activity in studies of NMR conditioning

in rabbits from other laboratories. Fig 10 shows an example where CR profiles from Fig 5 of Smith (1968) illustrated in panel A have been run back through a first-order model to generate the input profiles illustrated in panel B. Because only NMR data are available, the actual time constant of the best fit first-order filter cannot be determined. We instead used a value of 0.16 s which is the mean of the values found for RB 1-4 (see legend to Fig 6). The resulting input profiles could be well fitted with Gaussian curves, as could the EMG spike-frequency profiles in the present study (Fig 4). Both the peaks and widths of the Gaussian curves shown in Fig 10 vary with ISI (interval between CS and US onset in paired trials: actual data in Fig 10 from CS alone trials). The latency of the peak increases with ISI, as does the width of the curve. In addition, the height of the peak diminishes as the ISI increases.

Figure 11 about here

More details concerning the first two of these relationships are shown in Fig 11, for both the data from Smith (1968), and data from 4 additional studies (Coleman and Gormezano 1971; Millenson et al. 1977; Welsh 1992; Yeo et al. 1997). For each study, the conditioned NMR profiles were run backward through a range of simple models with time constants from 0.07 - 0.23 s (as in RB 1-4) and the predicted motoneuron signals fitted with Gaussian curves. The time of the peak of each Gaussian (relative to CS onset) is plotted against ISI in Fig 11A with error bars from the spread of time constants. The scatter plot is reasonably well fitted by a straight line, whose equation indicates that the time to peak of summed motoneuron activity is approximately the same as the ISI. This would be consistent with a wealth of data concerning CR timing. The time to peak of the inferred activity is also linearly related to its width (Fig 11B). The two equations for time to peak (Fig 11) can be combined to yield an expression that relates the onset latency λ of the activity to the ISI:

$$\lambda = (1 - 0.2\kappa)t_{isi} + \left(0.014\kappa - 0.02\right) \tag{16}$$

where κ denotes the number of standard deviations before the mean at which the activity is deemed to start, so that $\mu = \kappa\sigma/2+\lambda$. A starting criterion of 5% of peak amplitude corresponds to $\kappa \sim 2.5$, which gives

$$\lambda = 0.5\,t_{isi} + 0.015 \tag{17}$$

This expression indicates that the onset latency of the activity has two components, one fixed at ~15 ms, and a second related to the ISI (about half its value). As such it is broadly consistent with measurements summarized by Gormezano et al. (1983) indicating that "the frequency distribution of CR onset latencies is centered at about the midpoint of the CS-US interval" (p.216). It is of interest that although some data shown in Fig 11 were obtained with a counterweighted transducer (Coleman and Gormezano 1971; Millenson et al. 1977; Smith 1968), and some with a non-counterweighted transducer (Welsh 1992; Yeo et al. 1997), there appears to be no obvious difference between them.

Additional Observations

Data Analysis for Subject RB5

Analysis of EMG spikes for subject RB5 indicated that their peak frequency measured over 50 ms time (60 spikes/s, Fig 12E) was substantially lower than the peak frequencies found for RB1-4 (200-400 spikes/s shown in Fig 2), and that individual spikes all had similar temporal profiles as indicated by Principal Component Analysis (e.g. Stashuk 2001). It was therefore possible that in this particular subject the EMG electrode was recording primarily from a single motor unit, rather than from a number of units that would allow a reasonable estimate of motoneuron pool activity. Moreover, the CRs in RB5 tended to be either small (~2 mm) or large ~(8 mm), making it difficult to relate EMG parameters to CR parameters.

Figure 12 about here

RB5's data set, however, did allow examination of firing rate variability (possibly in a single unit) for very similar CRs (Fig 12). Panels A-D show examples of EMG spike trains for CRs with roughly similar amplitudes and temporal profiles. The variation in spike trains between trials is striking, as is the finding that when the trains are pooled over trials with similar CR profiles (n=18, panel E), their frequency distribution could be fitted with a Gaussian shaped curve as could the data for subjects RB1-4 (Fig 4). The question arises of how the putative Gaussian input signal (panel E) could produce the highly variable spike outputs shown in panels A-D. The mechanism appears not to be a simple Poisson process, because as illustrated in Panel F the best-fit Poisson distribution underestimates the frequency of very short interspike intervals (< ~50 ms). Inspection of the data suggests that these short interspike intervals correspond to brief bursts (2-4 spikes) which occur ~20% of the times a single spike would be expected from a Poisson process. Whether these bursts

arise from noisy inputs to a single motoneuron, or from multiple motoneurons, remains to be determined.

Spectral Analysis of NMR

Although the present study is concerned with conditioned responses of the nictitating membrane, the claim that external eyelid responses are driven by a high-frequency neural oscillator, running at 8 Hz in rabbit (Gruart et al. 2000) and 20 Hz in cat (Domingo et al. 1997), is of relevance if both conditioned nictitating membrane and external eyelid responses are driven by a common cerebellar command. We therefore investigated whether there is evidence for similar input oscillations in the present data. Since the spike trains extracted from the RB EMG records were noisy, we used instead the inferred force records generated by equation (12) and illustrated in Fig 9. Power spectra were determined from the Fast Fourier Transforms of the inferred force records of subjects RB1-5, and were found to contain no consistent peaks across subjects apart from that at 0 Hz to be expected from Gaussian input (data not shown). Above 10 Hz the spectra indicated the presence of high-frequency noise in amounts that varied from subject to subject.

Analyses of eyelid records had assumed force was simply proportional to acceleration (Domingo et al. 1997; Gruart et al. 2000), and so had examined the power spectra of acceleration profiles. We therefore also checked acceleration profiles from the present data (even though for a first-order model acceleration cannot be simply related to force input) to see whether evidence for oscillations could be found. As might be expected, differentiating the position traces greatly increased the effects of high-frequency noise (c.f. Welsh 1992, Fig 1) above 10 Hz, but no consistent peaks were found below 10 Hz.

It appears therefore that the present data provide no evidence for a neural oscillator in the control of the rabbit's NMR. There are a number of possible reasons for this apparent discrepancy with the eyelid data. One is that the oscillations actually arise from particular mechanical properties of the eyelid (plus recording coil) itself, which are not shared with the NMR. Another is that the actual NM mechanics, as represented by first-order plant with time constant of 0.1 s, would attenuate an 8 Hz component in the input by a factor of ~6 in comparison with low-frequency (< 0.5 Hz) components, so that its presence would be hard to detect. Thirdly, an analysis of conditioned eyelid responses in rabbits after section of the facial nerve suggested that "the oscillatory component recorded from eyelid

responses comes mainly from the facial motor system" (Leal-Campanario et al. 2004, p.1552), i.e. not from the retractor bulbi component. Finally, the discrepancy might have arisen because of procedural differences, for example in recording technology or in data processing and analysis.

DISCUSSION

The purpose of the present study was to examine the relation between the firing patterns of the accessory abducens motoneuron population and the temporal profiles of conditioned NMRs, in order to see to what extent in NMR conditioning the cerebellum is presented with a simplified 'virtual plant' that is easy to control. Population motoneuron firing was estimated by spike extraction from the EMG of the retractor bulbi muscle, and found to have a Gaussian profile (plus tail) whose height varied linearly with the amplitude of the conditioned response. Moreover, the relationship between individual EMG spikes and the NMR could be approximated by a first-order linear filter. These results were shown to be compatible (Figs 7 and 8) with the behavior of a detailed non-linear model of the retractor bulbi muscle and orbital tissues,provided motor units were recruited appropriately (Mavritsaki et al. 2007). Application of the first order model to data from a range of previous studies suggested that these CRs also were produced by summed motoneuron firing with a Gaussian profile, whose width and peak latency varied with interstimulus interval. These results strongly suggest that the cerebellum deals with a virtual plant that substantially simplifies control of CR amplitude and timing in NMR conditioning.

Methodological Issues

The difficulties of extracting motor unit action potential (MUAP) trains from the EMG are well known (e.g. Christodoulou and Pattichis 1999; Farina et al. 2001; Lewicki 1998; Loudon et al. 1992; e.g. McGill and Dorfman 1985; Stashuk 2001). Nevertheless, we avoided one of the major problems, namely the variations in MUAP shape and amplitude that make it difficult to classify MUAPs according to the motor unit of origin, because our objective was to estimate total MUAP activity, not the firing characteristics of individual motor units. The main methodological problem for the present study was whether simple spike extraction from the EMG provided a good estimate of the number of summed MUAPs. Experimental investigations have indicated that the soleus EMG can indeed behave as the simple algebraic sum of MUAPs (Day and Hulliger 2001) at least up until a certain level of muscle activity. We attempted to assess whether this was also true for the EMG records produced by our retractor bulbi electrodes, and concluded that the maximum spike rates obtained were still within the linear range. Moreover, insofar as synchronization would be a source of bias in estimating total MUAP activity (Day and Hulliger 2001), the evidence of substantial trial to trial variability in spike timing from

a putative single motor unit (Fig 12) suggests it is unlikely to be a major concern when the motor response of interest is the conditioned NMR.

Relation to Previous Data

The conditioned NMRs recorded here are similar to those obtained in previous studies (e.g. Gormezano et al. 1983), with respect to both temporal profile (including the long 'tail' denoting a slow return to resting position lasting ~1 s) and maximum amplitude of 2-8 mm (Garcia et al. 2003; Millenson et al. 1977; Welsh 1992; Yeo et al. 1997). The relatively modest change in the shape of the CR profile with increases in CR amplitude is also consistent with previous reports of conditioned NMR and eyelid profiles. These indicate that during acquisition there are (i) slight reductions in onset latency (Gormezano et al. 1983; Gruart et al. 1995; Schneiderman 1966; Schneiderman and Gormezano 1964; Smith 1968; Smith et al. 1969), though there appears to be great variability between the latencies of individual CRs early in acquisition (Frey and Ross 1968; Garcia et al. 2003; Schneiderman 1966; Schneiderman and Gormezano 1964; Smith et al. 1969), and (ii) no consistent change in peak latency (Gruart et al. 1995; Gruart et al. 2000; Leal-Campanario et al. 2004; Smith 1968; Welsh 1992). Thus, in general terms, the conditioned NMRs recorded here are representative, and this is confirmed by the finding that a model derived from them can also be applied to data from other laboratories (Fig 11).

As far as relations between CR profiles and EMG activity in the RB muscle are concerned, there appear to be very few previous data, possibly because of the technical difficulties of electrode implantation in this muscle in combination with the recording of NM position during conditioning. Thus Berthier (1992) shows only a single record of NM position and RB EMG. The present results constitute, to the best of our knowledge, the first systematic description of RB EMG during conditioning.

There have, however, been previous reports that indirectly support there being a close and possibly linear relation between summed RB motor unit firing and CR temporal profiles. First, activity in the EMG of the orbicularis oculi (OO) muscle is highly correlated with conditioned NMR amplitude (Lavond et al. 1990; McCormick et al. 1982), to such an extent that some studies use OO EMG activity as a measure of conditioning in its own right (e.g. Ivarsson and Svensson 2000; e.g. Mauk and Thompson 1987; Skelton 1988). Secondly, there have been a number of reports suggesting

linear relationships between aspects of OO EMG activity and the size and velocity of unconditioned blink responses (e.g. Evinger et al. 1991; Gruart et al. 1995; e.g. Manning and Evinger 1986; VanderWerf et al. 2003). Finally single unit recordings of activity in the motoneurons that innervate the OO muscle have suggested a linear relationship between their firing rate and the position of the eyelid for CRs (Trigo et al. 1999, Fig 16), and between firing rate and lid velocity for URs (Trigo et al. 1999, Fig 5). It may be recalled that for a first-order linear plant, input is related to a combination of position *and* velocity of output (e.g. equation (15)). However, for slow movements the position term will dominate the relationship, and for fast movements the velocity term will predominate. In the data reported by Trigo, Gruart and Delgardo-García (1999) the URs were rapid (peak velocities up to 700 deg/s) whereas the CRs, produced by trace conditioning with a brief airpuff CS, were almost an order of magnitude slower (peak velocities ~ 80 deg/s). Simulations show that our first-order model can produce the relationships between input signal and lid movement for both the URs and CRs illustrated in Figs 5 and 16 of Trigo et al. (1999) (results shown in Fig 13).

Figure 13 about here

Mechanisms for Linearisation

At first sight it is hard to reconcile the complexities of skeletal muscle and orbital mechanics with the simple linear model shown in Fig 7. In general terms, however, the NMR is a very stereotyped movement, which by always operating against the same load from the same starting position, and following only a somewhat loosely specified trajectory, utilizes just a small fraction of the full muscle repertoire. It is the kind of response that can typically be approximated by simple muscle models (e.g. Zahalak 1992).

More specifically, there are a number of mechanisms that could in principle contribute to NMR linearisation. Over the sub-maximal range of NMR amplitudes observed in the present study, the non-linearities apparent in isometric force production by the RB muscle (Mavritsaki et al. 2007, Fig 4c) are reduced when the muscle is allowed to shorten. Secondly, both the low-pass filtering action of the plant and the use of Gaussian input signals attenuates some of the high-frequency dynamic non-linearities produced by muscle activation. Thirdly, the use of noisy input signals over an appropriate frequency range has a linearising effect. The first two mechanisms particularly contribute to the ability

of the non-linear model to approximate the data obtained in the present experiment even in rate-coding-mode (results not shown).

As shown previously, appropriate recruitment of RB motor units provides a robust linearising mechanism over the full response range (Mavritsaki et al. 2007), and for the present data this recruitment allows the complex non-linear model to behave similarly to a simple first-order model (Figs 7, 8). Combined rate-coding and recruitment, and the recruitment of motor units in order of increasing strength, are strategies widely used both in skeletal muscle control (see Mavritsaki et al. 2007) and so are plausible mechanisms to create response linearization. Furthermore, preliminary analysis of spike amplitudes from the present EMG records suggests a close relationship between amplitude and inferred muscle force (Lepora et al. 2006), consistent with a recruitment strategy.

In summary, there are a number of mechanisms that could plausibly contribute towards linearising control of such a simple movement as the NMR. The fact that the present analysis indicates linearisation takes place does not therefore provide on its own unequivocal evidence for any particular mechanism. Nevertheless, there are a variety of reasons to believe that recruitment of motor units in the RB muscle is likely to play an important role.

Nature of Control Signal

The present results suggest that the control signal sent to the accessory abducens nucleus for a conditioned NMR produces an overall Gaussian-shaped increase in excitatory drive (with tail) that approximates the desired increase in muscle force produced by the RB muscle. The peak of the Gaussian is timed to coincide roughly with US onset, and its width increases linearly with the duration of the interval between CS and US onsets. The relation between the input signal and NM movement can be approximated by a first order differential equation (15), identical in form to that linking the firing of ocular motoneurons to rotatory eye movement (Keller 1981) under restricted conditions (Sklavos et al. 2005). Could such an input signal be generated in a straightforward manner by appropriate increases in the firing rates of the neurons in the interpositus nucleus as assumed in many models of eyeblink conditioning (e.g. Balkenius and Morén 1999; Fiala et al. 1996; Garenne and Chauvet 2004; Gluck et al. 2001; Hofstötter et al. 2002; Medina and Mauk 2000; Moore and Choi 1997)?

There appear to be at least two issues to be resolved before such a scheme could be accepted. First, while some blink-related neurons in the interpositus nucleus show the expected

behavior at least qualitatively (e.g. Aksenov et al. 2004; Berthier et al. 1991; Berthier and Moore 1990; Choi and Moore 2003; Freeman and Nicholson 2000; e.g. McCormick and Thompson 1984), others do not (e.g Delgado-García and Gruart 2005). It is possible that these differences arise because the the former experiments recorded primarily from the anterior interpositus nucleus, which has been , implicated by lesion and inactivation studies in the production of CRs, whereas the latter recorded primarily from the posterior interpositus nucleus, which has not been implicated in CR production. Such an interpretation would be broadly consistent with recent evidence on the firing patterns of neurons in the interpositus nucleus in relation to unconditioned blinks, which has led to the suggestion that there are at least two functionally distinct groups of blink-related neurons in the interpositus nucleus (Chen and Evinger 2006). However, a full understanding of the role of interpositus neurons in conditioning requires quantitative measures of the relationship between firing rate and CR parameters for individual neurons in the interpositus nucleus, and a determination of how such measures are correlated with the neurons' efferent and afferent connections. Such experiments are an important task for future research.

Secondly, the interpositus nucleus does not project directly to accessory abducens neurons, but via relay structures such as the red nucleus (Hesslow and Yeo 2002; Thompson 2005). Although the red nucleus appears to be a critical link in the pathway for expressing CRs, little known about its signal-processing role. For example, since interpositus neurons fire tonically but accessory abducens neurons do not, it is possible that an appropriate transformation takes place in the red nucleus. This suggestion could be consistent with recordings from red nucleus neurons indicating that some units do have baseline activity but others do not (Desmond and Moore 1991), but it is clear further data are needed. The issue of signal processing in the red nucleus is likely to be an important one for future models.

Two additional points concerned control signals for CRs need to be made. The first is that the linearised plant described in the present study would be of use to all structures sending signals to the accessory abducens nucleus for the production of conditioned NMRs, perhaps for example the hippocampus in trace conditioning. The second concerns an implication of the general view that the EMGs in the retractor bulbi and orbicularis oculi during CRs are similar. It might be the case that the eyelid plant also can be approximated by a first order linear filter, as indeed the results shown in Fig 13 begin to suggest. If so, a linearized plant could also be of use for the production of eyelid

responses, for example by cerebellar, hippocampal and cortical inputs. However, to understand the linearization process it would be necessary to construct a detailed model of the eyelid plant, using available information from detailed recordings of orbicularis oculi motoneurons during conditioned eyelid responses (e.g. Trigo et al. 1999).

Plant Simplification in Motor Control

Finally, the general principle of plant simplification addressed in the present study appears to have rather widespread application in biological motor control. For example, it has been suggested that the stretch reflex serves to linearise skeletal muscle responses (Nichols and Houk 1976), and that spinal cord circuitry is organised to allow linear summation of multiple inputs (Mussa-Ivaldi et al. 1994). An example of particular recent interest concerns the organisation of the oculomotor plant for eye rotations, where the claim that soft tissue pulleys greatly simplify both static and dynamic control has been vigorously debated (e.g. Angelaki and Hess 2004; Demer 2006; Klier et al. 2006; Porrill et al. 2000). The apparent existence of multiple mechanisms for simplifying the plant, for example the use of the stretch reflex where it is available for skeletal muscle, but reliance on recruitment in the NMR where the stretch reflex is not available for the retractor bulbi muscle, would be consistent with the importance of the process. Adequate characterisation of plant simplification may be an essential precursor to understanding the tasks confronting high-level neural controllers.

ACKNOWLEDGEMENTS

This research was supported by the UK Biotechnology and Biological Sciences Research Council (grant BBS/B/17026 under the Integrative Analysis of Brain and Behavior Initiative, and a Research Committee studentship to E.M.), and the National Eye Institute (EY07391 to C.E.).

References

Aksenov D, Serdyukova N, Irwin K, and Bracha V. GABA neurotransmission in the cerebellar interposed nuclei: Involvement in classically conditioned eyeblinks and neuronal activity. *J Neurophysiol* 91: 719-727, 2004.

Angelaki DE and Hess BJM. Control of eye orientation: where does the brain's role end and the muscle's begin? *Eur J Neurosci* 19: 1-10, 2004.

Balkenius C and Morén J. Dynamics of a classical conditioning model. *Auton Robots* 7: 41-56, 1999.

Bartha GT and Thompson RF. Control of rabbit nictitating membrane movements: 1. A computer model of the retractor bulbi muscle and the associated orbital mechanics. *Biol Cybern* 68: 135-143, 1992a.

Bartha GT and Thompson RF. Control of rabbit nictitating membrane movements: II. Analysis of the relation of motoneuron activity to behavior. *Biol Cybern* 68: 145-154, 1992b.

Berthier NE. Muscle activity during unconditioned and conditioned eye blinks in the rabbit. *Behav Brain Res* 48: 21-28, 1992.

Berthier NE, Barto AG, and Moore JW. Linear systems analysis of the relationship between firing of deep cerebellar neurons and the classically conditioned nictitating membrane response in rabbits. *Biol Cybern* 65: 99-106, 1991.

Berthier NE and Moore JW. Activity of deep cerebellar nuclear cells during classical conditioning of nictitating membrane extension in rabbits. *Exp Brain Res* 83: 44-54, 1990.

Berthier NE and Moore JW. The nictitating membrane response: An electrophysiological study of the abducens nerve and nucleus and the accessory abducens nucleus in rabbit. *Brain Res* 258: 201-210, 1983.

Cegavske CF, Patterson MM, and Thompson RF. Neuronal unit activity in the abducens nucleus during classical conditioning of the nictitating membrane response in the rabbit. *J comp physiol Psychol* 93: 595-609, 1979.

Chen FP and Evinger C. Cerebellar modulation of trigeminal reflex blinks: interpositus neurons. *J Neurosci* 26: 10569-10576, 2006.

Choi JS and Moore JW. Cerebellar neuronal activity expresses the complex topography of conditioned eyeblink responses. *Behav Neurosci* 117: 1211-1219, 2003.

Christodoulou CI and Pattichis CS. Unsupervised pattern recognition for the classification of EMG signals. *IEEE Trans Biomed Eng* 46: 169-178, 1999.

Coleman SR and Gormezano I. Classical conditioning of the rabbit's (*Oryctolagus cuniculus*) nictitating membrane response under symmetrical CS-US interval shifts. *J comp physiol Psychol* 77: 447-455, 1971.

Day SJ and Hulliger M. Experimental simulation of cat electromyogram: Evidence for algebraic summation of motor-unit action-potential trains. *J Neurophysiol* 86: 2144-2158, 2001.

Delgado-García JM and Gruart A. Firing activities of identified posterior interpositus nucleus neurons during associative learning in behaving cats. *Brain Res Rev* 49: 367-376, 2005.

Demer JL. Evidence supporting extraocular muscle pulleys: Refuting the platygean view of extraocular muscle mechanics. *J Pediatr Ophthalmol Strabismus* 43: 296-305, 2006.

Desmond JE and Moore JW. Single-unit activity in red nucleus during the classically-conditioned rabbit nictitating-membrane response. *Neurosci Res* 10: 260-279, 1991.

Disterhoft JF, Quinn KJ, Weiss C, and Shipley MT. Accessory abducens nucleus and conditioned eye retraction/nictitating membrane extension in the rabbit. *J Neurosci* 5: 941-950, 1985.

Disterhoft JF and Weiss C. Motoneuronal control of eye retraction/nictitating membrane extension in rabbit. In: *Neural Mechanisms of Conditioning*, edited by Alkon DL and Woody CD. New York: Plenum, 1985, p. 197-208.

Domingo JA, Gruart A, and Delgado-García JM. Quantal organization of reflex and conditioned eyelid responses. *J Neurophysiol* 78: 2518-2530, 1997.

Eglitis I. The glands. In: *The Rabbit in Eye Research*, edited by Prince JH. Springfield, Il: Charles C. Thomas, 1964, p. 38-56.

Evinger C, Manning KA, and Sibony PA. Eyelid movements. Mechanisms and normal data. *Invest Ophthal Vis Sci* 32: 387-400, 1991.

Farina D, Colombo R, Merletti R, and Olsen HB. Evaluation of intra-muscular EMG signal decomposition algorithms. *J Electromyogr Kinesiol* 11: 175-187, 2001.

Fiala JC, Grossberg S, and Bullock D. Metabotropic glutamate receptor activation in cerebellar Purkinje cells as substrate for adaptive timing of the classically conditioned eye-blink response. *J Neurosci* 16: 3760-3774, 1996.

Freeman JH and Nicholson DA. Developmental changes in eye-blink conditioning and neuronal activity in the cerebellar interpositus nucleus. *J Neurosci* 20: 813-819, 2000.

Frey PW and Ross LE. Classical conditioning of the rabbit eyelid response as a function of the interstimulus interval. *J comp physiol Psychol* 65: 246-250, 1968.

Garcia KS, Mauk MD, Weidemann G, and Kehoe EJ. Covariation of alternative measures of responding in rabbit (*Oryctolagus cuniculus*) eyeblink conditioning during acquisition training and tone generalization. *Behav Neurosci* 117: 292-303, 2003.

Garenne A and Chauvet GA. A discrete approach for a model of temporal learning by the cerebellum: in silico classical conditioning of the eyeblink reflex. *J integ Neurosci* 3: 301-318, 2004.

Gluck MA, Allen MT, Myers CE, and Thompson RF. Cerebellar substrates for error correction in motor conditioning. *Neurobiol Learn Mem* 76: 314-341, 2001.

Gormezano I, Kehoe EK, and Marshall BS. Twenty years of classical conditioning research with the rabbit. In: *Progress in Psychobiology and Physiological Psychology*, edited by Sprague JM and Epstein AN: Academic Press, 1983, p. 197-275.

Gruart A, Blázquez P, and Delgado-García JM. Kinematics of spontaneous, reflex, and conditioned eyelid movements in the alert cat. *J Neurophysiol* 74: 226-248, 1995.

Gruart A, Schreurs BG, Del Toro ED, and Delgado-García JM. Kinetic and frequency-domain properties of reflex and conditioned eyelid responses in the rabbit. *J Neurophysiol* 83: 836-852, 2000.

Gruart A and Yeo CH. Cerebellar cortex and eyeblink conditioning - bilateral regulation of conditioned responses. *Exp Brain Res* 104: 431-448, 1995.

Hesslow G and Yeo CH. The functional anatomy of skeletal conditioning. In: *A Neuroscientist's Guide to Classical Conditioning*, edited by Moore JW. New York: Springer, 2002, p. 86-146.

Hofstötter C, Mintz M, and Verschure PFMJ. The cerebellum in action: a simulation and robotics study. *Eur J Neurosci* 16: 1361-1376, 2002.

Ivarsson M and Svensson P. Conditioned eyeblink response consists of two distinct components. *J Neurophysiol* 83: 796-807, 2000.

Keller EL. Oculomotor neuron behavior. In: *Models of Oculomotor Behavior and Control*, edited by Zuber BL. Boca Raton, Florida: CRC Press, 1981, p. 1-19.

Klier EM, Meng H, and Angelaki DE. Three-dimensional kinematics at the level of the oculomotor plant. *J Neurosci* 26: 2732-2737, 2006.

Lavond DG, Logan CG, Sohn JH, Garner WDA, and Kanzawa SA. Lesions of the cerebellar interpositus nucleus abolish both nictitating membrane and eyelid EMG conditioned responses. *Brain Res* 514: 238-248, 1990.

Leal-Campanario R, Barradas-Bribiescas JA, Delgado-García JM, and Gruart A. Relative contributions of eyelid and eye-retraction motor systems to reflex and classically conditioned blink responses in the rabbit. *J Appl Physiol* 96: 1541-1554, 2004.

Lennerstrand G. Mechanical studies on the retractor bulbi muscle and its motor units in the cat. *J Physiol* 236: 43-55, 1974.

Lepora NF, Mavritsaki E, Porrill J, Dean P, Yeo CH, and Evinger LC. Evidence for linearity in control of nictitating membrane responses by retractor bulbi motor units. In: *2005 Abstract Viewer/Itinerary Planner*. Washington, DC: Society for Neuroscience, 2005, Prog. No. 869.3.

Lepora NF, Porrill J, Dean P, Yeo CH, and Evinger LC. Simple recruitment model describes control of conditioned nictitating membrane response by retractor bulbi muscle. In: *2006 Abstract Viewer/Itinerary Planner*. Washington, DC: Society for Neuroscience, 2006, Prog. No. 345.16.

Lewicki MS. A review of methods for spike sorting: the detection and classification of neural action potentials. *Network: Computation in Neural Systems* 9: R53-R78, 1998.

Loudon GH, Jones NB, and Sehmi AS. New signal processing techniques for the decomposition of EMG signals. *Medical & Biological Engineering & Computing* 30: 591-599, 1992.

Manning KA and Evinger C. Different forms of blinks and their two-stage control. *Exp Brain Res* 64: 579-588, 1986.

Mauk MD and Thompson RF. Retention of classically conditioned eyelid responses following acute decerebration. *Brain Res* 403: 89-95, 1987.

Mavritsaki E, Lepora NF, Porrill J, Yeo CH, and Dean P. Response linearity determined by recruitment strategy in detailed model of nictitating membrane control. *Biol Cybern* 96: 39-57, 2007.

Mavritsaki E, Porrill J, Ivarsson M, Yeo CH, and Dean P. Recruitment of retractor bulbi motor units in a population model of the nictitating membrane response. *Soc Neurosci Abstr* 27: Prog. no. 405.4, 2001.

McCormick DA, Lavond DG, and Thompson RF. Concomitant classical conditioning of the rabbit nictitating membrane and eyelid responses: correlations and implications. *Physiol Behav* 28: 769-775, 1982.

McCormick DA and Thompson RF. Neuronal responses of the rabbit cerebellum during acquisition and performance of a classically conditioned nictitating membrane-eyelid response. *J Neurosci* 4: 2811-2822, 1984.

McGill KC and Dorfman LJ. Automatic decomposition electromyography (ADEMG): Validation and normative data in brachial biceps. *EEG Clin Neurophys* 61: 453-461, 1985.

Medina JF and Mauk MD. Computer simulation of cerebellar information processing. *Nat Neurosci* 3: 1205-1211, 2000.

Millenson JR, Kehoe EJ, and Gormezano I. Classical-conditioning of rabbit's nictitating-membrane response under fixed and mixed CS-US intervals. *Learn Motiv* 8: 351-366, 1977.

Moore JW and Choi JS. Conditioned response timing and integration in the cerebellum. *Learning & Memory* 4: 116-129, 1997.

Mussa-Ivaldi FA, Giszter SF, and Bizzi E. Linear combinations of primitives in vertebrate motor control. *Proc Natl Acad Sci USA* 91: 7534-7538, 1994.

Nichols TR and Houk JC. Improvement in linearity and regulation of stiffness that results from actions of stretch reflex. *J Neurophysiol* 39: 119-142, 1976.

Porrill J, Warren PA, and Dean P. A simple control law generates Listing's positions in a detailed model of the extraocular muscle system. *Vis Res* 40: 3743-3758, 2000.

Sanders DB, Stalberg EV, and Nandedkar SD. Analysis of the electromyographic interference pattern. *J Clin Neurophysiol* 13: 385-400, 1996.

Schneiderman N. Interstimulus interval function of nictitating membrane response of rabbit under delay versus trace conditioning. *J comp physiol Psychol* 62: 397-402, 1966.

Schneiderman N and Gormezano I. Conditioning of nictitating membrane of rabbit as function of CS-US interval. *J comp physiol Psychol* 57: 188-195, 1964.

Skelton RW. Bilateral cerebellar lesions disrupt conditioned eyelid responses in unrestrained rats. *Behav Neurosci* 102: 586-590, 1988.

Sklavos S, Porrill J, Kaneko CRS, and Dean P. Evidence for a wide range of time scales in oculomotor plant dynamics: Implications for models of eye-movement control. *Vis Res* 45: 1525-1542, 2005.

Smith MC. CS-US interval and US intensity in classical conditioning of the rabbit's nictitating membrane response. *J comp physiol Psychol* 66: 679-687, 1968.

Smith MC, Coleman SR, and Gormezano I. Classical conditioning of the rabbit's nictitating membrane response at backward, simultaneous, and forward CS-US intervals. *J comp physiol Psychol* 69: 226-231, 1969.

Stashuk D. EMG signal decomposition: how can it be accomplished and used? *J Electromyogr Kinesiol* 11: 151-173, 2001.

Thompson RF. In search of memory traces. *Ann Rev Psychol* 56: 1-23, 2005.

Trigo JA, Gruart A, and Delgado-García JM. Discharge profiles of abducens, accessory abducens, and orbicularis oculi motoneurons during reflex and conditioned blinks in alert cats. *J Neurophysiol* 81: 1666-1684, 1999.

VanderWerf F, Brassinga P, Reits D, Aramideh M, and deVisser BO. Eyelid movements: Behavioral studies of blinking in humans under different stimulus conditions. *J Neurophysiol* 89: 2784-2796, 2003.

Welsh JP. Changes in the motor pattern of learned and unlearned responses following cerebellar lesions: a kinematic analysis of the nictitating membrane reflex. *Neurosci* 47: 1-19, 1992.

Yeo CH, Hardiman MJ, and Glickstein M. Classical conditioning of the nictitating membrane response of the rabbit. I. Lesions of the cerebellar nuclei. *Exp Brain Res* 60: 87-98, 1985.

Yeo CH, Lobo DH, and Baum A. Acquisition of a new-latency conditioned nictitating membrane response - major, but not complete, dependence on the ipsilateral cerebellum. *Learn Mem* 3: 557-577, 1997.

Zahalak GI. An overview of muscle modelling. In: *Neural Prostheses: Replacing Motor Function after Injury or Disease*, edited by Stein RB, Peckam PH and Popovic´ DB. New York: Oxford University Press, 1992, p. 17-57.

Figure 1

Example of spike extraction from EMG of retractor bulbi muscle (subject RB 4).

A Portion of EMG record shown with expanded time base, to illustrate threshold crossing criterion for spike extraction.

B The entire EMG record for a CS alone trial (middle trace), showing extracted spikes (bottom trace), and the conditioned nictitating membrane response (top trace). Vertical line shows time of US onset. Since CS onset is at time zero, the interstimulus interval (ISI) was 350 ms.

Figure 2

Records of retractor bulbi EMG spike frequency and conditioned nictitating membrane responses (CRs) for subjects RB 1-4. Each panel shows the averaged records from the largest 20% of CRs for an individual subject. US onset denoted by vertical dotted line, CS onset at time zero. Interstimulus interval (ISI) therefore 500 ms for RB 1, 350 ms otherwise. EMG frequencies calculated over 50 ms bins at 10 ms intervals (e.g. 1-50, 11-60 ms and so on).

Figure 3

Change in CR profile with amplitude for subjects RB 1-4.

In each panel CS onset is at time zero, and US onset denoted by the dotted vertical line. Each trace is the mean of 3 CRs, chosen to reflect the full amplitude range for each subject.

Figure 4

Change in EMG frequency profiles with peak frequency for subjects RB 1-4.

In each panel CS onset is at time zero, and US onset denoted by the dotted vertical line. Each trace is the mean of three EMG frequency profiles, where an individual profile was calculated every 10 ms as the frequency of extracted spikes in the previous 50 ms bin. The profiles correspond to the CR traces shown in Fig 3. Gaussian curves were fitted to the traces as described in Methods. The peak times of the Gaussians, measured relative to US onset, were for each subject in order RB 1-4: -110 to -10 ms, -80 to +60 ms, -100 to +70 ms, -60 to 0 ms. For each subject the largest sigma values for the Gaussians were 160, 70, 160 and 90 ms.

Figure 5

Relation between peak CR amplitude and peak EMG frequency for subjects RB 1-4.

Panels A-D: Each data point corresponds to mean CR and EMG values for 3 conditioned responses. Also shown are the lines of best fit, and r^2 values where r is the correlation coefficient.

Panel E: Relation of spike threshold to linearity. The grey line in each graph illustrates for that subject how choice of spike threshold influenced the intercept of the best-fit line. The intercept is large either for threshold values that are too low, allowing spikes unrelated to CR production (noise) to be counted as signal, or are too high, allowing spikes related to CR production (signal) to be counted as noise. The dotted line shows the values of threshold chosen (0.17, 0.15, 0.0275 and 0.0375 mV for RB 1-4). The black line in each graph shows how the r^2 value measuring goodness of linear fit varied with threshold for each subject. In all cases the r^2 values were high for a wide range of threshold values.

Figure 6

Examples of observed and fitted CR profiles for subjects RB 1-4.

In each panel the traces labeled 'Experiment' are the mean of 3 CR profiles (pooled on the basis of amplitude -see text); for each individual CR profile the corresponding EMG spikes were run through the best-fit first-order linear filter. The trace labeled 'Linear model fit' is the mean of the 3 corresponding filter outputs. Filter time constants for the subjects in order RB 1 to 4 were 0.22, 0.14, 0.23 and 0.07 seconds and filter gains were 0.06, 0.10, 0.11 and 0.26. The traces shown produced the median R^2 value (proportion of variance accounted for) for each subject. The lower confidence limits (above which 95% of the R^2 values lay) for each subject in order RB 1 to 4 were 0.94, 0.79, 0.97 and 0.94.

Figure 7

Detailed and simplified models of NMR production by motoneuron firing.

Top row: block diagram of Bartha and Thompson's (1992a; 1992b), re-implemented by Mavritsaki et al. (2007). Inputs to the model are the firing patterns of 100 motoneurons, each passed through a nonlinear model of isometric force production. The summed isometric force then drives a model of the

orbital mechanics via a nonlinear model of muscle dynamics that takes muscle length and velocity into account. The output of the orbital-mechanics model is the NMR.

Bottom row: simplified linear model based on best-fit linear filter. Input to the model is the summed firing patterns of the motoneurons. This procedure produces a notional muscle force via a simple gain, which then acts on a first-order linear plant to produce the NMR.

Figure 8

Performance of detailed NMR model with a Gaussian-shaped input profile.

A: Comparison of peak amplitudes between NMR model linearised by a combination of recruitment and frequency modulation, and that with only frequency modulation.

B: Example of first order linear filter (time constant 0.1 s, gain 0.12) fit to the input-output data for detailed model. Data fitted across the range of responses in panel A for recruitment and frequency modulation.

Figure 9

Examples of observed EMG frequency profiles and estimated force profiles for subjects RB 1-4.

In each panel the trace labeled 'Frequency data' is the mean of 3 recorded EMG spike frequency profiles, pooled on the basis of amplitude. Each of the 3 corresponding CR profiles was run backward through the simplified linear model (Fig 7) to generate estimated muscle force; the mean of the 3 force estimates is labeled 'Force F data (the dimensions of this trace are mm/s, because it is normalised by a proportionality constant with the dimensions of viscosity - see text). The traces shown produced the median R^2 value (proportion of variance accounted for) indicated for each subject. The lower confidence limits (above which 95% of the R^2 values lay) for each subject in order RB 1 to 4 were 0.73, 0.74, 0.80 and 0.84.

Figure 10

Example of simplified model applied to data from the study by Smith (1968).

A: Profiles of conditioned NMRs obtained by training at different intervals (ISIs) between CS onset and US onset (redrawn from bottom row of Fig 5 of Smith (1968)). The trace corresponding to an ISI

of 1000 ms has been excluded, on the grounds of possible forebrain involvement in such long intervals, and consequent uncertainty concerning the nature of control signal.

B: Reconstructed input signals for the CR profiles in panel A, obtained by passing the CR profiles back through the first-order model with time constant 0.16 s (see text).

Figure 11

Properties of reconstructed control signals for conditioned rabbit NMRs from 5 previous studies for a range of simple models with time constants from 0.07 to 0.23 s..

A: Time from CS onset to the peak of the reconstructed Gaussian control signal (μ) versus ISI duration (t_{isi}) is well fitted by a straight line with the equation

$$\mu = t_{isi} - 0.02 \tag{18}$$

where times are in seconds.

B: Width of the Gaussian control signal σ versus its mean μ fitted by straight line with equation

$$\sigma = 0.4\mu - 0.02 \tag{19}$$

(units are seconds).

Figure 12

RB 5: variation in EMG spike trains corresponding to similar CR profiles.

A-D: Four examples of spike trains and CR profiles.

E: Frequency distribution for EMG spike trains pooled over 18 trials all with similar CR profiles, together with best-fit Gaussian curve. Frequencies calculated from number of spikes in successive 50 ms bins.

F: Distribution of inter-spike intervals over 18 trials. Smooth curve shows best-fit Poisson distribution which clearly underestimates the number of short (< 50 ms) interspike intervals. The histogram is better fitted by a lognormal distribution with expected value 16 ms and standard deviation 36 ms (not shown).

Figure 13

Relation of simulated motoneuron firing rate to position and velocity during fast and slow movements for first order plant model.

Gaussian input profiles appropriate to either a fast or slow movement were applied to a first-order filter (time constant 0.1 s). Data points were obtained from the instantaneous values of position or velocity and input signal at 1 ms intervals throughout the movement. Only points with input signal values greater than the equivalent of 10 deg/s were plotted. The position values were perturbed by low-amplitude white noise (mean = 0 deg, SD = 0.02 deg), and the position records low-pass filtered at 50 Hz.

A & B: Fast movement (peak velocity 360 deg/s) generated by Gaussian input signal with height assigned a value of 360 sp/s and width σ=10 ms. Resultant movement has similar early-phase parameters to those of the eyelid URs analyzed in Fig 5 of Trigo et al. (1999). Points taken from start of movement to its peak amplitude.

C & D: Slow movement (peak velocity 80 deg/s) generated by Gaussian input signal with height equivalent to 75 sp/s and width 80 ms. Resultant movement has similar characteristics to the eyelid CRs analyzed in Fig 16 of Trigo et al. (1999). Points taken from start of movement to peak of input signal.

Figure 1

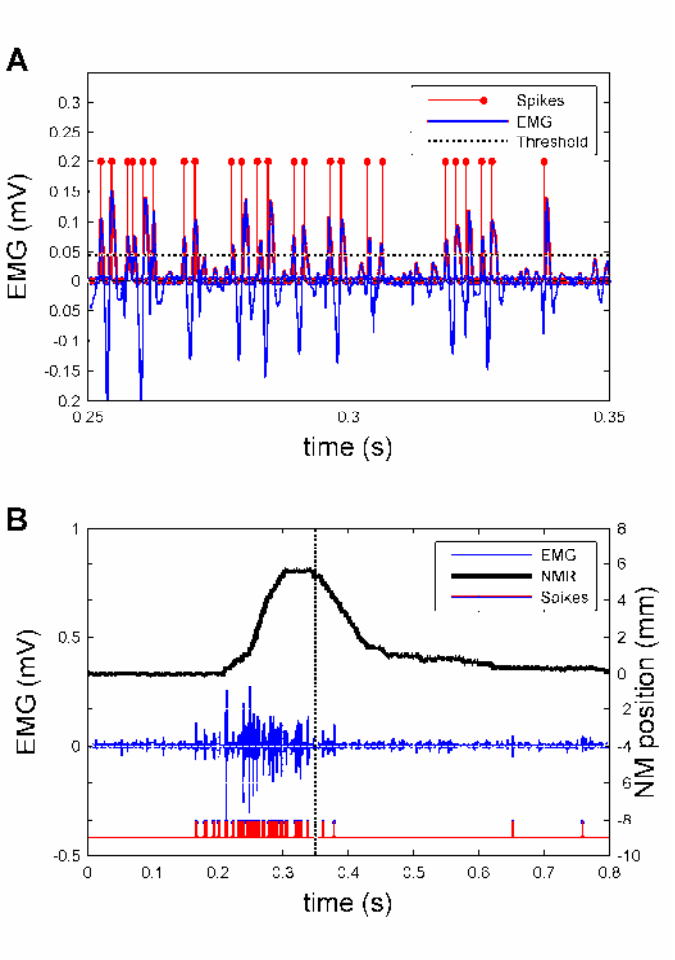
A
Spikes
EMG
Threshold
EMG (mV)
time (s)
B
EMG
NMR
Spikes
EMG (mV)
NM position (mm)
time (s)

Figure 2

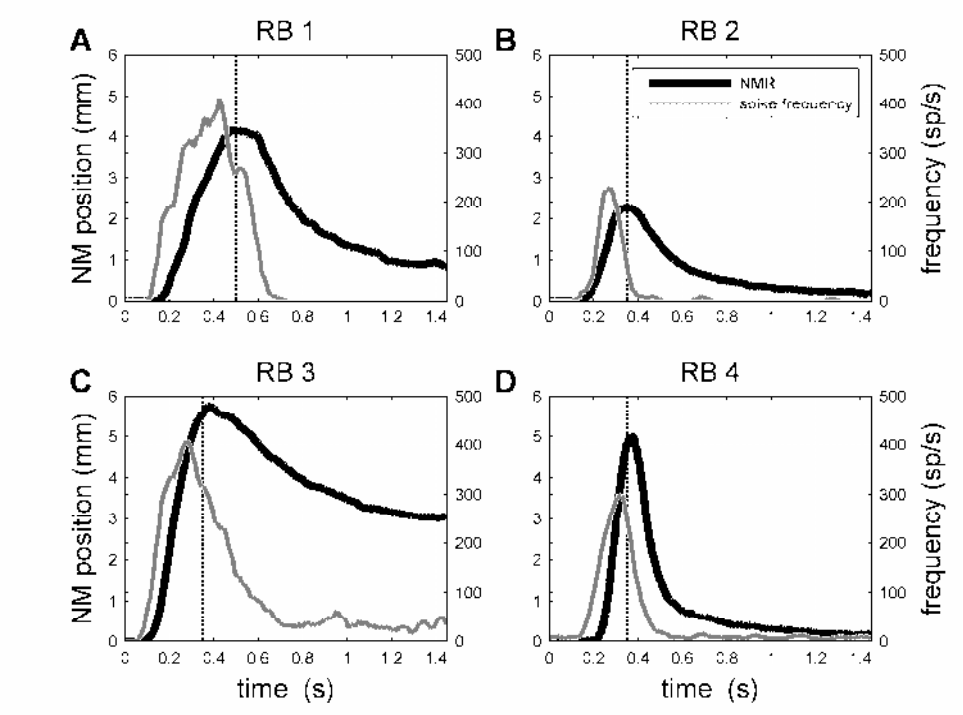
A
RB 1
B
RB 2
NMR
spike frequency
C
RB 3
D
RB 4
NM position (mm)
frequency (sp/s)
time (s)

Figure 3

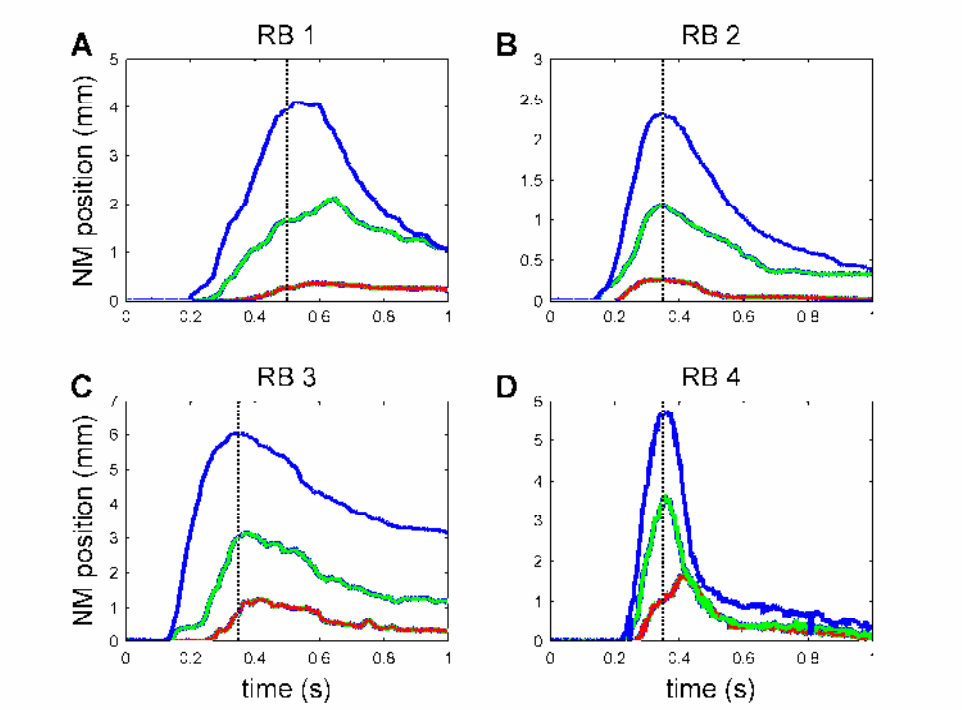
A
RB 1
B
RB 2
C
RB 3
D
RB 4
NM position (mm)
NM position (mm)
time (s)
time (s)

Figure 4

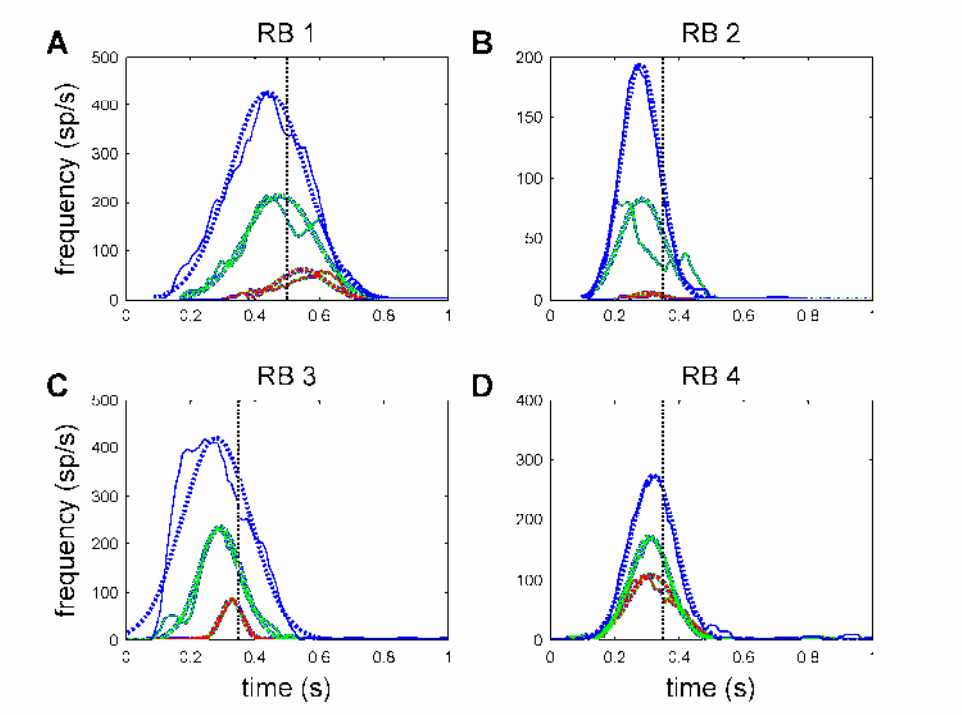
A
RB 1
B
RB 2
C
RB 3
D
RB 4
frequency (sp/s)
frequency (sp/s)
time (s)
time (s)

Figure 5

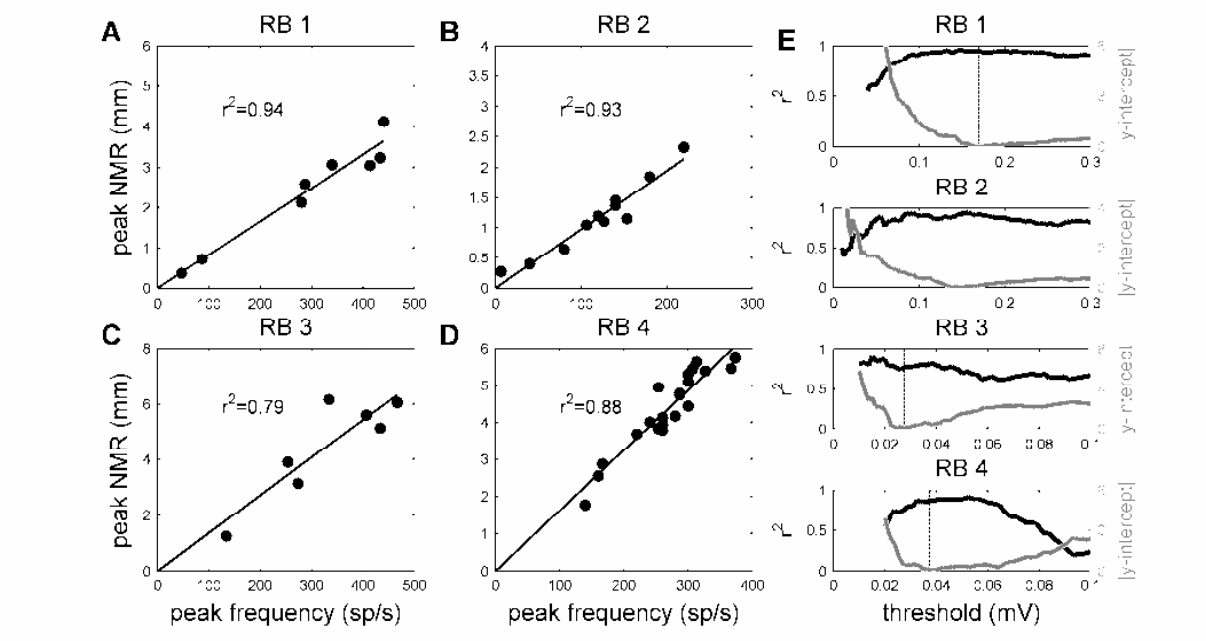
A
RB 1
r²=0.94
peak NMR (mm)
B
RB 2
r²=0.93
C
RB 3
r²=0.79
peak NMR (mm)
peak frequency (sp/s)
D
RB 4
r²=0.88
peak frequency (sp/s)
E
RB 1
RB 2
RB 3
RB 4
r²
|y-intercept|
threshold (mV)

Figure 6

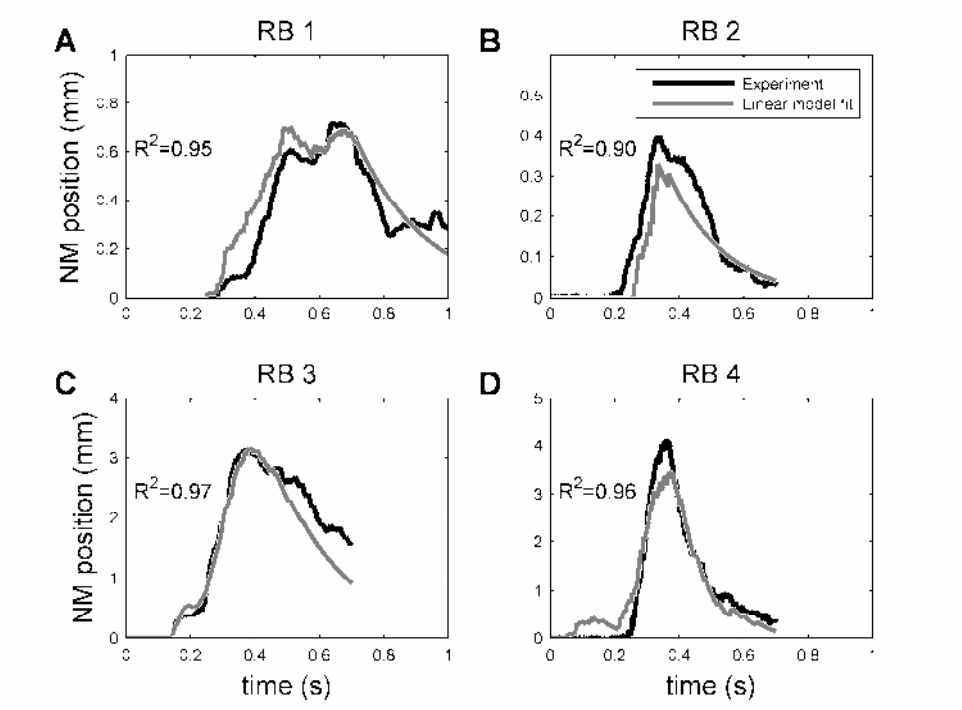
A
RB 1
NM position (mm)
R2=0.95
B
RB 2
Experiment
Linear model fit
R2=0.90
C
RB 3
NM position (mm)
R2=0.97
time (s)
D
RB 4
R2=0.96
time (s)

Figure 7

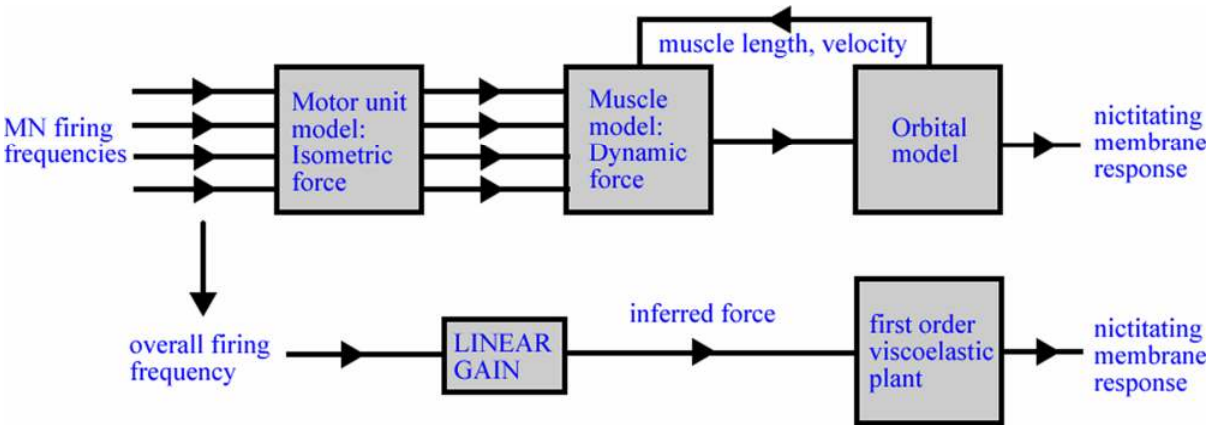
muscle length, velocity
MN firing frequencies
Motor unit model: Isometric force
Muscle model: Dynamic force
Orbital model
nictitating membrane response
overall firing frequency
LINEAR GAIN
inferred force
first order viscoelastic plant
nictitating membrane response

Figure 8

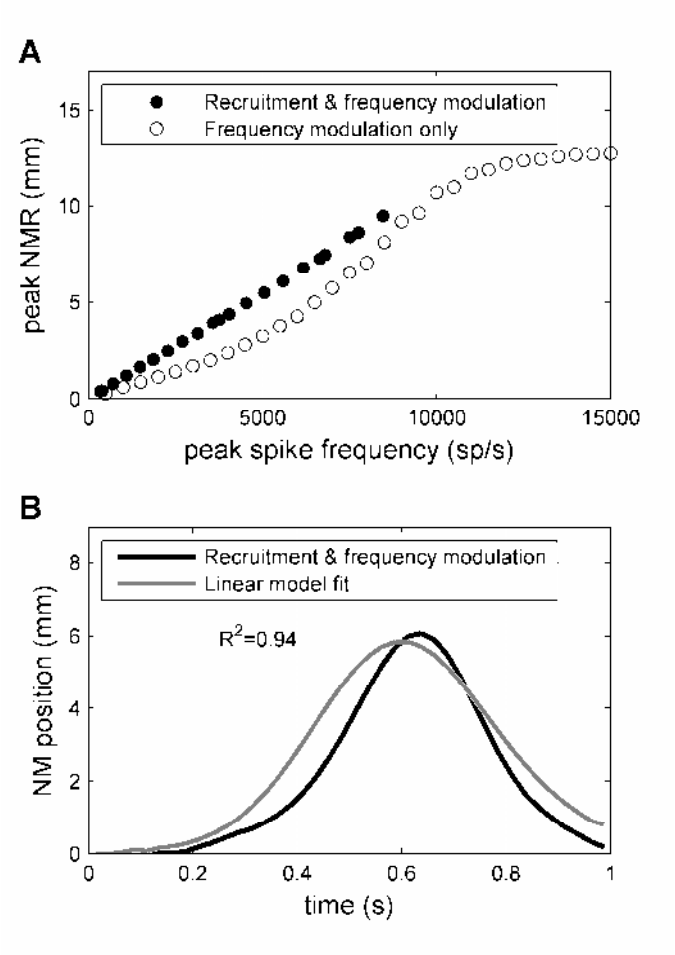
A
Recruitment & frequency modulation
Frequency modulation only
peak NMR (mm)
peak spike frequency (sp/s)
0
5
10
15
0
5000
10000
15000
B
Recruitment & frequency modulation
Linear model fit
R^2=0.94
NM position (mm)
time (s)
0
2
4
6
8
0
0.2
0.4
0.6
0.8
1

Figure 9

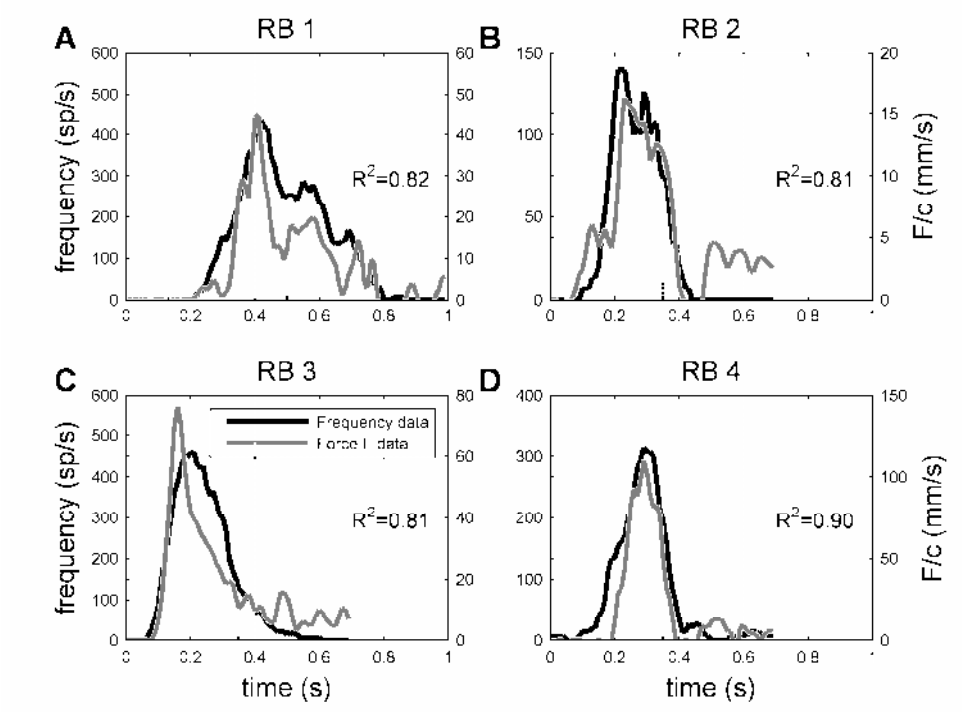
A
RB 1
B
RB 2
C
RB 3
D
RB 4
frequency (sp/s)
F/c (mm/s)
time (s)
R^2=0.82
R^2=0.81
R^2=0.81
R^2=0.90
Frequency data

Figure 10

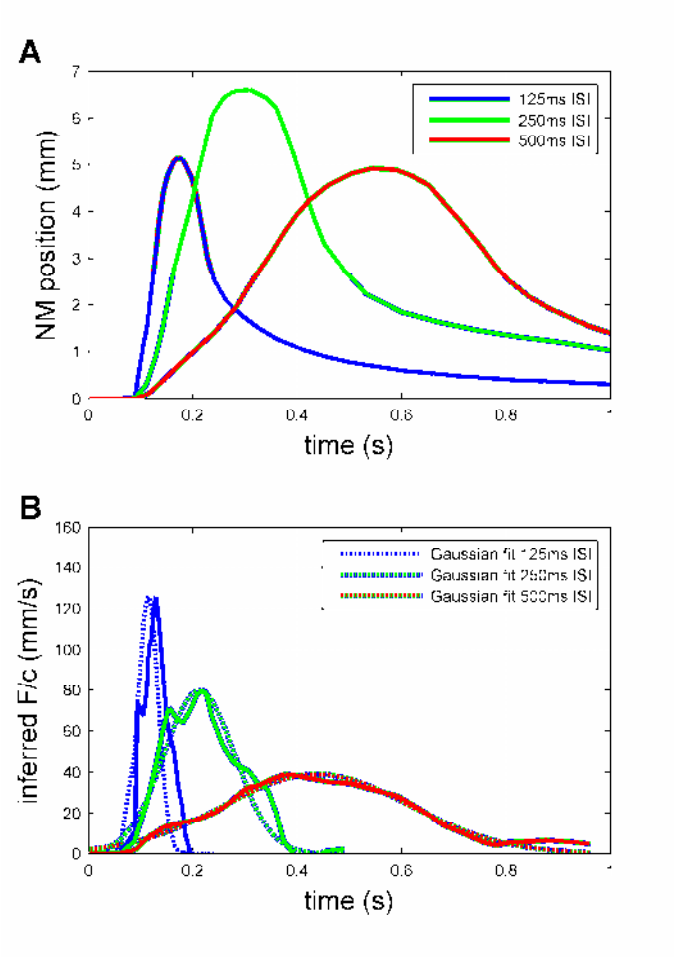
A
NM position (mm)
time (s)
125ms ISI
250ms ISI
500ms ISI
B
inferred F/c (mm/s)
time (s)
Gaussian fit 125ms ISI
Gaussian fit 250ms ISI
Gaussian fit 500ms ISI

Figure 11

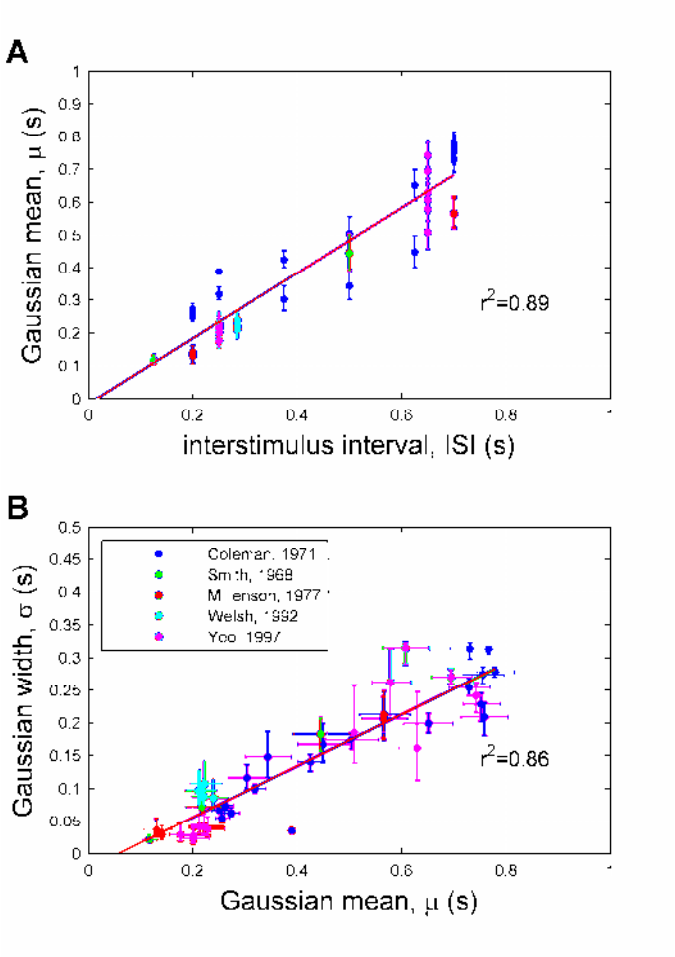
A
Gaussian mean, μ (s)
interstimulus interval, ISI (s)
r²=0.89
B
Gaussian width, σ (s)
Gaussian mean, μ (s)
r²=0.86

Figure 12

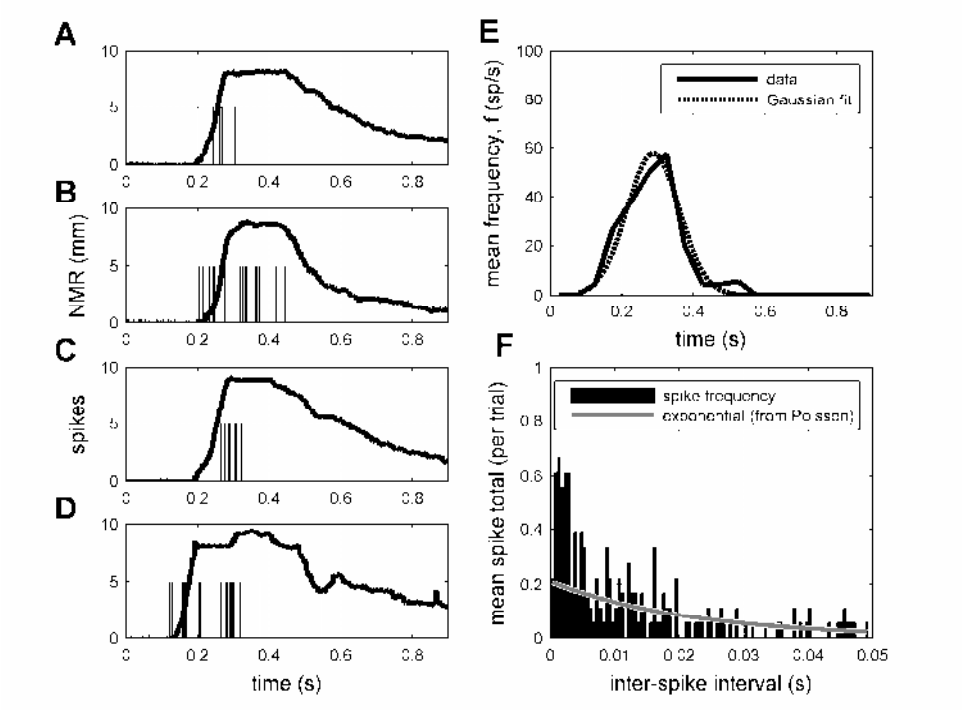
A
B
C
D
NMR (mm)
spikes
time (s)
E
F
mean frequency, f (sp/s)
data
Gaussian fit
time (s)
mean spike total (per trial)
spike frequency
exponential (from Poisson)
inter-spike interval (s)

Figure 13

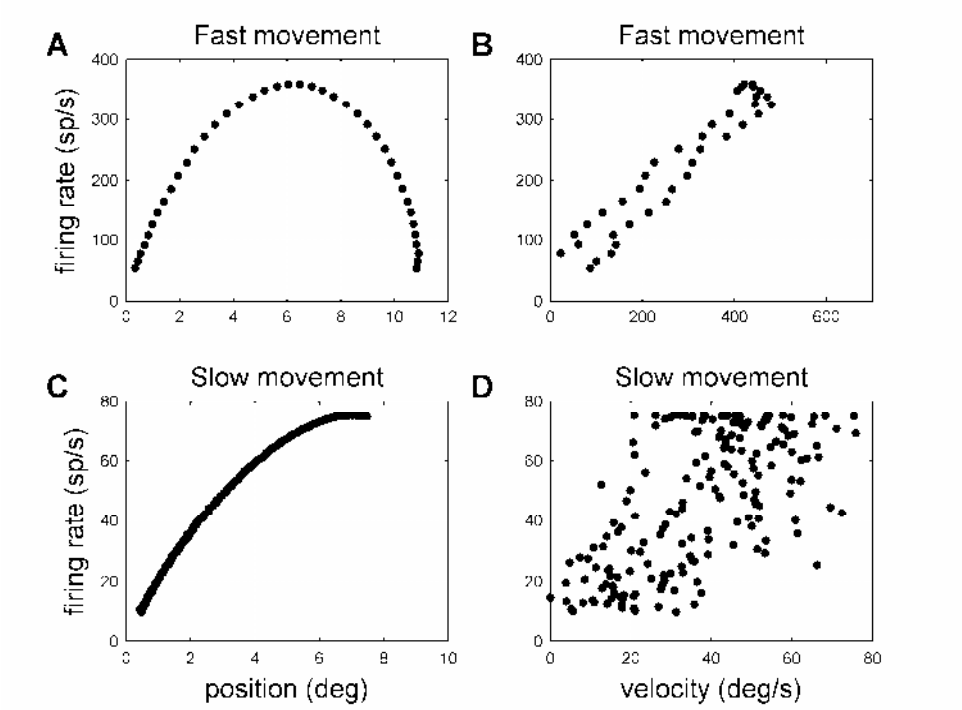
A
Fast movement
firing rate (sp/s)
B
Fast movement
C
Slow movement
firing rate (sp/s)
position (deg)
D
Slow movement
velocity (deg/s)